Proceedings of the 2006 IEEE
International Conference on Control Applications
Munich, Germany, October 4-6, 2006

Using Force Control for Fidelity in Low-Force Medical Haptic Simulators

Kostas Vlachos and Evangelos Papadopoulos, *Senior Member, IEEE*

***Abstract*—In this paper the effect of force control in the fidelity of a low-force five degree-of-freedom (dof) haptic mechanism is investigated. Strict conditions that guarantee stability are presented. Our effort focuses on haptic devices, able to reproduce accurate low forces in a soft virtual environment, rather than large forces in stiff virtual environments. Open and closed loop controllers are applied to a haptic mechanism, which is a part of a training medical simulator for urological operations, and consists of a two-dof, five bar linkage and a three-dof spherical joint. The force control algorithm is described and discussed. Open and closed loop schemes are compared. Simulation and experimental results of the force control law applied to the five-dof mechanism are presented and discussed. It is shown that the use of closed loop force control law increases the haptic device fidelity and the realism of the simulation. It is also shown that in case of haptic devices used in soft virtual environments, issues like signal noise and device stiffness are more critical than maintaining system stability.**

I. Introduction

VIRTUAL Reality is now an accepted tool in areas ranging from mechanical design to entertainment and medical training. During the past several years, research on improving the virtual environment realism has introduced the haptic devices, [1]. The fidelity of a haptic device is often measured by its transparency characteristics. Transparency is associated with the absence of haptic device-induced parasitic torques/forces during its motion, e.g. mass/inertia, gravity forces and friction. Transparency is even more important for haptic devices used in simulators, where reality must be simulated reliably. There are two ways to maximize transparency, (a) optimized design resulting in haptic mechanisms with minimum device-induced parasitic torques/forces, and (b) use of a closed loop control law. Most closed loop control laws designed for haptic devices are used with hard virtual environments, aiming at securing stability, and at maximizing fidelity.

Minsky *et al.* used an impedance controller for a haptic joystick and presented a relationship between sampling rate, virtual environment stiffness, damping and the system stability, [2]. A PID force control law is presented by Birglen *et al.* to control the 3-dof haptic device SHaDe, [3]. Carignan and Cleary investigated several control methodologies, [4]. Furthermore, an adaptive control scheme using active observers was proposed by Cortesão *et al.*, [5].

Colgate *et al.* presented the use of a virtual coupling between the haptic mechanism and the virtual environment and the necessary coupling conditions for system stability, [6]. A virtual coupling consisting of a virtual spring-damper using a "god-object" approach was introduced by Zilles and Salisbury, [7]. Adams and Hannaford used the "two-port framework", a method rooted in linear circuit theory, to solve the problem of stable haptic simulation, [8, 9]. Gil *et al.* applied the Routh-Hurwitz criterion to study the stability of a 1-dof haptic device, [10]. Hannaford and Ryu used an energy-based method to guarantee system stability, using a "Passivity Observer" and a "Passivity Controller", [11]. Methods trying to guarantee system stability independently from the virtual environment give rather conservative results, and sometimes require additional computational load. On the other hand, Miller *et al.* investigated how to design a virtual environment to guarantee stability, [12].

In this paper, the effect of force control in the fidelity of a low-force haptic mechanism is investigated. The paper makes novel contributions in two areas. First, it studies techniques that increase the fidelity of haptic devices, designed to reproduce accurate *low* forces in *soft* virtual environments, rather than *large* forces in *stiff* virtual environments. Second, using the Routh-Hurwitz criterion, it identifies new stability conditions that are stricter than those in [2], [6], and [10]. As an example, a 5-dof haptic device, designed to reproduce low forces in soft virtual environments is used. Open and closed loop force control is described, simulated, experimentally studied, and compared. The closed loop system exhibits a substantially improved response with respect to the open loop system. It was found that in contrast to devices designed for use with stiff virtual environments, where stability issues are a main concern, in low-force haptic mechanisms, mechanism stiffness and system noise determine the quality of the simulator.

II. Brief Description of The Haptic Mechanism

The haptic mechanism employed here, is part of a training simulator for minimal invasion urological operations, [13]. In short, during a minimal invasion urological operation on a male patient, a surgeon moves the tip of an endoscope along the patient urethra to the bladder, via an intermediate point. At this point, the endoscope orientation changes without translation, so as to align the entire urethra and continue the insertion without traumas. During the main operation, the endoscope rotates in all directions but its tip translates minimally. These observations reveal the fact that although

Manuscript received February 10, 2006. This work is co-funded by the European Social Fund (75%) and National Resources (25%)-(EPEAEK II)-PYTHAGORAS.

K. Vlachos and E. Papadopoulos are with the Department of Mechanical Engineering, National Technical University of Athens, 15780 Athens, Greece, (e-mail: {kostaswl; egpapado}@central.ntua.gr).

the endoscope can have any orientation in a cone, its tip translations occur on the plane of symmetry of the patient and thus a haptic mechanism with two translational and three rotational dof is needed, [13].

The quality of a haptic device is often measured by its transparency characteristics. A great effort was placed in developing an optimum haptic mechanism, i.e. one with the best mechanical design under given kinematical, operational and constructional constraints, [14]. However, although optimization is required and must always be employed first, it cannot eliminate completely devise parasitic forces and torques so as to achieve perfect transparency. In principle, this can be done using a control strategy that compensates for all parasitic terms. However, in practice this is hard to achieve due to the difficulty of identifying accurately all terms contributing to the parasitic terms. In addition, such a practice results in larger motors and inertias. The hypothesis raised in this paper is that a combination of the optimization and control approaches may further enhance the performance of a haptic device.

III. Control Of A Haptic Device

A. Open Loop Control

We consider first the open loop control case, where coreless DC motors actuate the device and apply torques to create the feeling that only the endoscope and the tissues are present. To compute the necessary motor currents, the equations of motion of the surgical tool during a real surgical operation, see the box in Fig. 1, are written as

$$\mathbf{M}_t \dot{\mathbf{v}}_{cm} + \mathbf{V}_t + \mathbf{G}_t = \mathbf{F} + \mathbf{F}_r \tag{1}$$

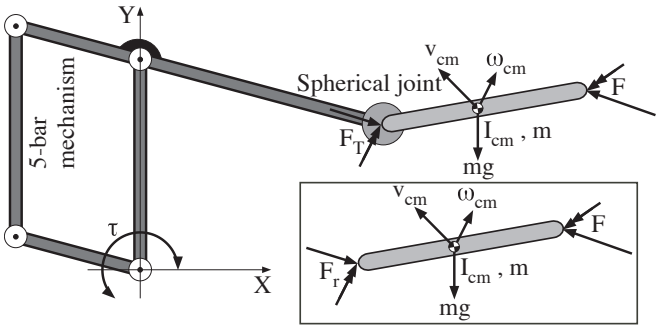

Fig. 1. Forces on surgical tool during a real surgical operation (figure in the box) and a simulated surgical operation, where the endoscope in attached at the haptic mechanism.

where $\mathbf{F}$ is the vector of forces and torques applied by the operator to the tool, $\mathbf{M}_t$ is the tool mass matrix, $\mathbf{V}_t$ contains velocity terms, $\mathbf{G}_t$ contains gravity terms, and $\mathbf{v}_{cm}$ is the velocity of its center of mass. The vector $\mathbf{F}_r$ contains forces and torques, which are due to tissue deformation. Since no motion is allowed in the Z direction, in the virtual environment, $\mathbf{M}_t$ is a 5×5 matrix and the rest of the vectors have appropriate dimensions.

Furthermore, the equations of motion of the surgical tool attached to the haptic mechanism end effector during a simulated surgical operation, see Fig. 1, are written as

$$\mathbf{M}_t \dot{\mathbf{v}}_{cm} + \mathbf{V}_t + \mathbf{G}_t = \mathbf{F} + \mathbf{F}_T \tag{2}$$

The vector $\mathbf{F}_T$ contains forces and torques, applied by the haptic mechanism to the surgical tool. In order to build a transparent haptic device, the user must feel during the simulation the real forces and torques, that would be present in a real operation. In other words our goal is to find the vector $\boldsymbol{\tau}$ of actuators torques, so that vector $\mathbf{F}_T$ is equal vector $\mathbf{F}_r$. The equations of motion of the haptic mechanism during a simulated surgical operation are written as

$$\mathbf{M}_m \dot{\mathbf{v}} + \mathbf{V}_m + \mathbf{G}_m = \mathbf{J}^{-T}\boldsymbol{\tau} - \mathbf{F}_T \tag{3}$$

where $\mathbf{J}^{-T}\boldsymbol{\tau}$ is the vector of the applied torques by the actuators resolved as forces and torques at the end effector, $\mathbf{M}_m$ is the haptic mechanism mass matrix, $\mathbf{V}_m$ contains velocity terms, $\mathbf{G}_m$ contains gravity terms. Again, $\mathbf{M}_m$ is a 5×5 matrix and the rest of the vectors have appropriate dimensions. Replacing $\mathbf{F}_T$ with $\mathbf{F}_r$, (3) becomes

$$\mathbf{M}_m \dot{\mathbf{v}} + \mathbf{V}_m + \mathbf{G}_m = \mathbf{J}^{-T}\boldsymbol{\tau} - \mathbf{F}_r \tag{4}$$

From (4) we find that the required actuator torque vector $\boldsymbol{\tau}$ must be given by

$$\boldsymbol{\tau} = \mathbf{J}^T(\mathbf{M}_m \dot{\mathbf{v}} + \mathbf{V}_m + \mathbf{G}_m + \mathbf{F}_r) \tag{5}$$

In general, the forces and torques $\mathbf{F}_r$ are functions of the position and velocity of the tool and are computed based on a model of tissue deformation as

$$\mathbf{F}_r = \mathbf{F}_r(\dot{\mathbf{q}}, \mathbf{q}) \tag{6}$$

A detailed description of a simplified tissue model can be found in [15]. Using (5), the open loop control commands to the motor amplifiers are given by

$$\mathbf{u} = (\mathbf{K}_T \mathbf{K}_{amp})^{-1}\mathbf{J}^T(\mathbf{M}_m \dot{\mathbf{v}} + \mathbf{V}_m + \mathbf{G}_m + \mathbf{F}_r) \tag{7a}$$

where $\mathbf{K}_T$, and $\mathbf{K}_{amp}$ are diagonal matrices that contain motor torque constants and amplifier gains, respectively. Assuming small accelerations and velocities, and a balanced mechanism $\mathbf{M}_m \dot{\mathbf{v}}$, $\mathbf{V}_m$, and $\mathbf{G}_m$ are negligible. Then, the control command to the motor amplifiers are given by

$$\mathbf{u} = (\mathbf{K}_T \mathbf{K}_{amp})^{-1}\mathbf{J}^T\mathbf{F}_r \tag{7b}$$

In order to verify the above, we conducted open loop experiments and compared them with simulation runs. The results are described next.

1) Simulation

Two simulation scenarios are implemented. In the first one, the endoscope is displaced freely in a sinusoidal manner along the X-axis, without any contact with the virtual environment. The mathematical model of the haptic device

assuming a balanced mechanism, and including viscous and Coulomb friction forces, is the following,

$$\mathbf{F}_{sen} = \mathbf{F}_{act} - (\mathbf{M}_m \dot{\mathbf{v}} + \mathbf{V}_m + \mathbf{B}\mathbf{v} + \mathbf{C}\,\mathrm{sgn}(\mathbf{v})) \qquad (8)$$

where $\mathbf{F}_{sen}=\mathbf{F}_T$ is the forces and torques vector felt by the user, $\mathbf{F}_{act}=\mathbf{J}^{-T}\boldsymbol{\tau}$ is the vector of the actuated forces and torques from the motors to the user, and **B** and **C** are diagonal matrices of viscous friction coefficients and Coulomb friction forces respectively. Since our first simulation scenario is a free translation of the haptic device end-effector, and there is no tissue deformation, the command to the motor amplifiers is equal to zero according to (7b), and thus the sensed force $\mathbf{F}_{sen}$ should be the mechanism induced parasitic forces.

The first plot in Fig. 2 shows the induced force during the motion shown in the second graph. Velocity and acceleration are also presented in Fig. 2. In order to be able to compare simulated to experimental trials, the displacement input for the simulation runs is exactly the same to that of the experiments.

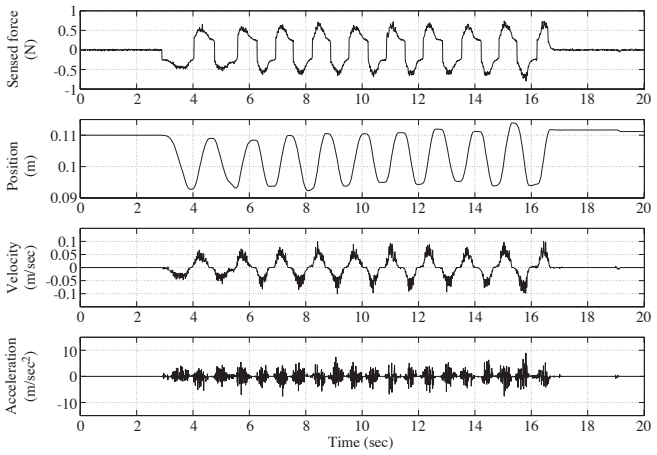

Fig. 2. Open loop for the first scenario simulation.

The simulation results show a value of device-induced parasitic forces along the X-axis of about ±0.6 N, which is unacceptable for a low-force haptic device.

In the second simulation scenario, the endoscope that is attached on the haptic device end-effector is translated along the X-axis, against a virtual human tissue, see Fig. 3.

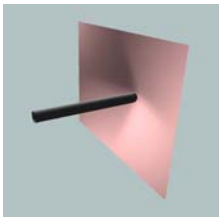

Fig. 3. Translation of the endoscope attached to the haptic device end-effector against a virtual human tissue.

In this case, since there is contact with the virtual environment, $\mathbf{F}_{act}$ is calculated according to the following simplified spring model of tissue deformation,

$$\mathbf{F}_{act} = \mathbf{k} \cdot \mathbf{x} \qquad (9)$$

where **k** is the spring constant vector, and **x** the translation and rotation vector of the end-effector.

Simulation results of this second case are shown in Fig. 4. Here, the endoscope translates for about 3 cm along the X-axis, until it reaches the virtual human tissue, and then it translates further for approximately 1 cm, see Fig. 3. The force that the user should feel is 1.12 N and is calculated according to (9), with the spring constant along the X-axis, k_x, equal to 125 N/m. As shown in Fig. 4c, there is an error of about 0.3 N. The small vibrations in Fig. 4 are due to the motion of the user hand as recorded during a real test session.

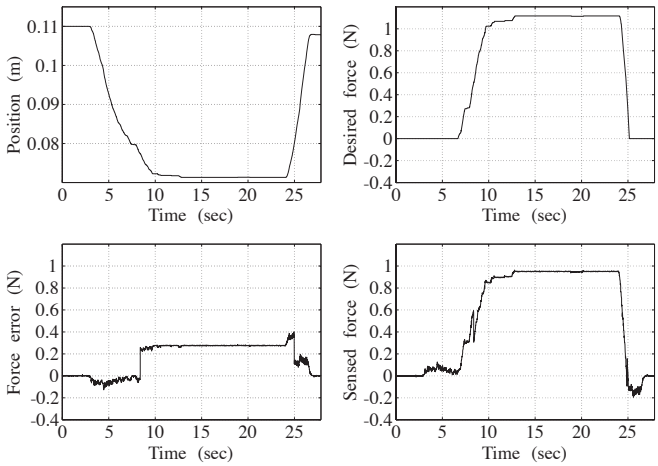

Fig. 4. Open loop for the second scenario simulation.

2) Experimentation

The above presented simulated scenarios are implemented also in the real haptic device. In order to measure the forces that the haptic device applies to the user, an ATI Nano 17 force/torque sensor is attached to the device end-effector, see Fig. 5, capable of 50 N in X, Y axes, 70 N in Z axis and 500 mNm around the three axes of full-scale loads. Its weight is only 0.01 kg. Special interfaces were developed to attach the sensor on the mechanism end-effector.

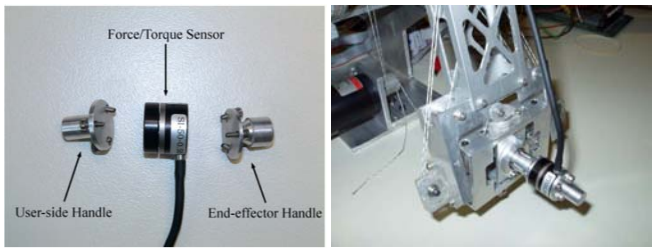

Fig. 5. Haptic mechanism end-effector with force/torque sensor.

Fig. 6 shows the experimentally measured force, the translation, velocity and acceleration during the first scenario, where the end-effector is moving freely in a sinusoidal manner along the X-axis without any contact with the virtual environment. The measured force is due to device-induced parasitic force, and the result is very close to the simulated one, see Fig. 2. Its value is about ±0.4 N.

Fig. 7 shows the measured force in the second scenario experiment, where the endoscope is translated for about 3

cm along the X-axis until the virtual human tissue is reached, and then it is translated further for 1 cm, see Fig. 3.

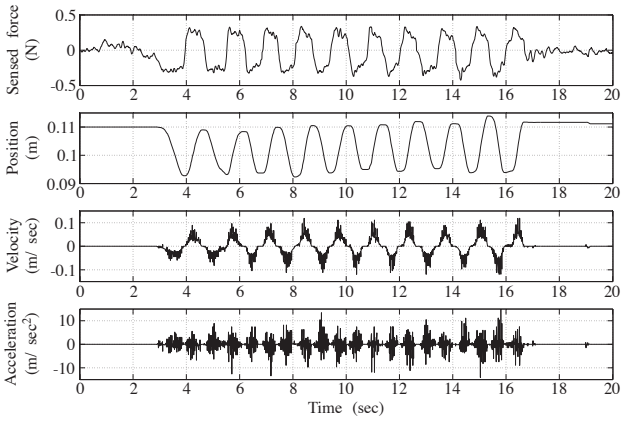

Fig. 6. Open loop for the first scenario experiment.

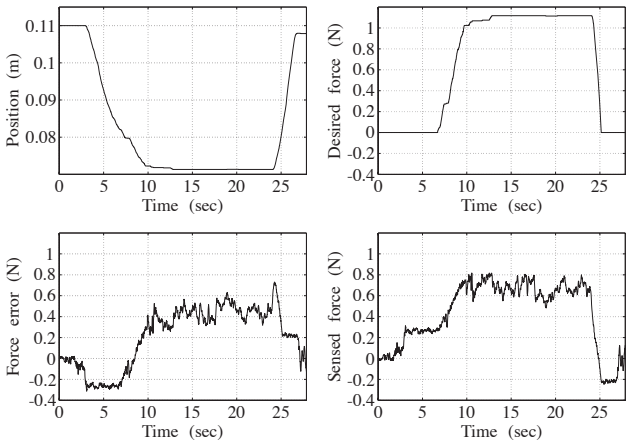

Fig. 7. Open loop for the second scenario experiment.

The desired force in Fig. 7 is the one calculated from the soft tissue model described in (9). The sensed force and the relative error are also given in Fig. 7. The desired force has a maximum of about 1.12 N, and the error of about 0.5 N. The results are very close to the simulated experiment. The chattering shown is due to hand tremor especially between 10 and 23 seconds, where the haptic device applies force against the user hand.

The above simulation and experimentation results shown that the haptic mechanism under open loop control cannot simulate reliably the virtual environment and is due to inertia and friction factors. In order to overcome this problem we develop a closed loop force control scheme.

B. Closed Loop Control

The closed loop force control block diagram is presented in Fig. 8. The desired value that our plant, the "haptic mechanism" block, should output is the desired force, $\mathbf{F}_{des}$, which is calculated in the "Virtual Environment" block according to (9). The error between the desired force, $\mathbf{F}_{des}$, and the force sensor output $\mathbf{F}_{sen}$, is $\mathbf{F}_{err}$, which is fed into the P "Controller" block. The sensor output is subject to noise.

The haptic mechanism input is then calculated according to the following control law

$$\mathbf{F}_{in} = \mathbf{F}_{des} + \mathbf{K}_p \mathbf{F}_{err} \tag{10}$$

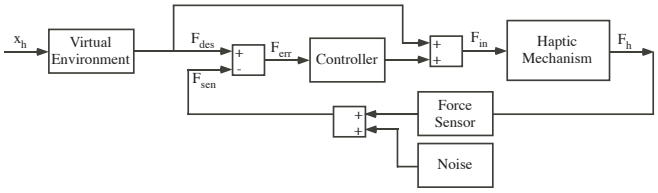

Fig. 8. Closed loop force control block diagram.

Replacing the desired force $\mathbf{F}_{des}$, with the virtual environment output according (9), The haptic mechanism input is the following

$$\mathbf{F}_{in} = \mathbf{k}\mathbf{x}_e + \mathbf{K}_p \mathbf{F}_{err} \tag{11}$$

Finally, the vector $\boldsymbol{\tau}$ of the actuators torques is the following

$$\boldsymbol{\tau} = \mathbf{J}^T(\mathbf{k}\mathbf{x}_e + \mathbf{K}_p \mathbf{F}_{err}) \tag{12}$$

We implemented the same simulation and experimental scenarios as in the open loop case, and the results are shown in Figs. 9 and 10. Fig 9 shows the first scenario results (simulation and experiment), i.e. the free sinusoidal motion of the end-effector without any contact with the virtual environment. The controller gain in the X-axis is equal to 5. The first plot shows the end-effector motion, which is the same for both the simulation and the experiment cases. The second plot displays the simulated scenario results and the third the experimental ones. Both in simulation and in actual experiment, the results are much better that those of the open loop. The sensed device induced parasitic forces are about 0.1 N that is a reduction of 80%.

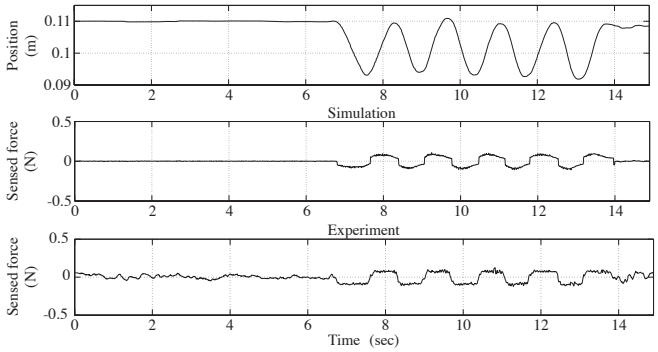

Fig. 9. Closed loop for the first scenario.

Fig 10 shows the second scenario results (simulation and experiment). The controller gain in the X-axis is equal to 5. The first pair of graphs shows the end-effector motion, which is the same for both the simulation and experiment cases, and the desired calculated force from the soft tissue model. The second graph pair shows the sensed and error force in the simulated scenario and the third the same forces in the experimental one. Again, the results are much better that those of the open loop. Here, the error force is about 0.1 N, i.e. an improvement of 66% compared to simulation and 80% compared to experimental results.

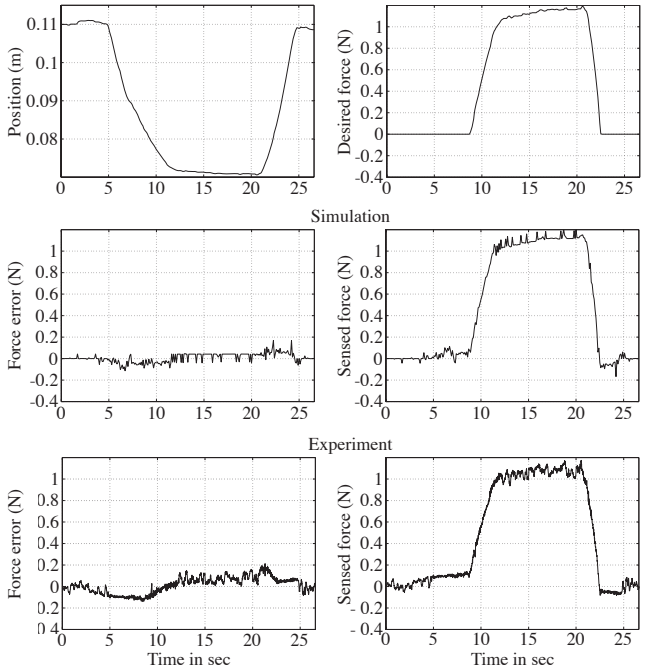

Fig. 10. Closed loop for the second scenario.

Table I presents the results of both types of control, which shows that the haptic mechanism under closed loop force control exhibits a substantially improved response with respect to the open loop system.

TABLE I
CLOSED AND OPEN LOOP CONTROL RESULTS

	Open loop	Closed loop	Improvement
First scenario force (simulation)	±0.6 N	±0.1 N	83%
First scenario force (experiment)	±0.4 N	±0.1 N	75%
Second scenario force error (simulation)	0.3 N	±0.1 N	66%
Second scenario force error (experiment)	0.5 N	0.2 N	60%

C. Discussion of the Results

As was seen in the previous section, closed loop force control improves significantly the fidelity of a medical haptic device. The improvement is even greater than what it Table I suggests, since one must subtract from the remaining force errors the threshold forces and moments that a human hand can feel. Therefore, in an actual experiment with a closed loop controller, the feel is better that what is expected from the table figures.

IV. CLOSED LOOP STABILITY

A question that normally arises when closed loop control is used, is whether the loop is stable and what are the limits for the closed loop bandwidth. Although our efforts focus on low-force haptic devices operating in soft virtual environments, the use of closed loop control requires a stability study of the closed loop system. A lot of work, some of which is referenced in the Introduction, has been devoted to the stability of haptic devices and the definition of some limits for the open or closed loop bandwidth.

In the closed loop control scheme we used, see Fig. 8, the Routh-Hurwitz criterion was employed, and the necessary limits for a stable closed loop were defined. The transfer function between the system input, i.e. the hand translation x_h, and the system output, i.e. the force that the user feels F_h, is given by.

$$F_h(s) / X_h(s) = (G_v^2 G_m(1+G_c)) / (1+(G_m G_v G_c H_s)) \quad (13)$$

where G_v is the Virtual Environment block transfer function, G_m is the Haptic Mechanism transfer function, G_c is the Controller transfer function and H_s is a delay in the feedback. Table II presents the various transfer functions, where K_v and B_v are the virtual environment spring and damper coefficients respectively, M_m and B_m are the haptic mechanism apparent mass and the mechanism damper coefficients respectively and T is the sample period.

TABLE II
BLOCK TRANSFER FUNCTIONS

Block	Transfer function
Virtual Environment, G_v	K_v+B_vs
Haptic Mechanism, G_m	$1/(M_ms^2+B_ms)$
Controller (P controller), G_c	K_p
Delay, H_s	$(2-Ts)/(2+Ts)$

Using the Routh-Hurwitz criterion we define conditions that guarantee the closed loop system stability. If we use a P controller (K_d=K_i=0), then the system is stable if both the following inequalities are true.

$$B_v < (2M_m + B_m T) / (K_p T) \quad (14)$$

$$K_v < Nom_p / Denom_p \quad (15)$$

where

$$Nom_p = 4B_m M_m + 4B_v K_p M_m + 2B_m{}^2 T - 2B_v{}^2 K_p{}^2 T$$
$$Denom_p = 4K_p M_m T + B_m K_p T^2 - B_v K_p{}^2 T^2$$

Equations (14) and (15) describe the limits of the virtual environment that the haptic mechanism can simulate and at the same time maintain its stability, assuming a P controller. Note here that these limits are more strict than those in previous works such as [10]. Similar limits, but far more complex, were derived for a PI, PD or PID controller. For example using a PI controller the system is stable if

$$\begin{aligned}&[(B_v < B_m / 3K_p) AND (K_v \le -\sqrt{A} + B)\\ &AND(K_i < C)] OR [(B_v < B_m / 3K_p) AND\\ &(-\sqrt{A} + B < K_v \le \sqrt{A} + B)\\ &AND(K_i < (2K_p K_v) / (-2B_v + K_v T))] OR\\ &[(B_v < B_m / 3K_p) AND (\sqrt{A} + B < K_v < 2B)\\ &AND(K_i < C)]\end{aligned} \quad (16)$$

or if

$$\begin{aligned}&(B_m / 3B_v \le K_p < (2M_m + B_m T) / (B_v T)) AND\\ &(K_v < 2B) AND (K_i < C)\end{aligned} \quad (17)$$

where

$$A = (B_m{}^2 - 2B_m B_v K_p - 3B_v{}^2 K_p{}^2) / (K_p{}^2 T^2)$$
$$B = (B_m + B_v K_p) / (K_p T)$$
$$C = (2B_m + 2B_v K_p - K_p K_v T) / (B_v T)$$

Based on our experiments, we found that M_m= 0.25 Kg and B_m= 5 Ns/m. Here, T=1 kHz and K_p= 5. According to the limits proposed in [10], the upper limit for the spring coefficient of the simulated environment is equal 2200 N/m. Using (14), we calculated that the upper limit for the spring coefficient of the simulated environment is equal 1105 N/m. In both cases, the limit exceeds by far the stiffness experienced in our application, which does not exceed 350 N/m, depending on virtual human tissue type and simulated pathology. This means that the above limits are more useful in stiff virtual environments, where sudden large forces appearing in a feedback loop as high gain terms, result in instabilities. However, in medical training applications like ours, where haptic devices are used, the forces tend to be low in magnitude and the environment tends to be soft.

This is not to say that limits to the achievable fidelity do not exist, but as we found in our experiments, in the analysis for low-force haptic devices in soft environments other factors must be taken into account. One such factor is the closed loop bandwidth that can be reached given that the device is designed to be lightweight and therefore not infinitely rigid. Via a mechanical stiffness experiment at the device tip, the lowest resonance of the mechanism was found experimentally to be equal to 193 Hz. Assuming a closed loop bandwidth 2 times lower than this frequency, the control loop gain upper limit is 11, while if the closed loop bandwidth is chosen as 5 times lower, the control gain limit is 5, i.e. equal to the one used in our experiments. Based on this analysis, one could try a gain in the range 5-10 and further reduce the force tracking error. However, it was found that this is not possible, because of another problem.

Indeed, increasing the gain K_p, the system becomes sensitive to the force/torque sensor noise, and the user starts feeling this noise at the endoscope. Since better sensors at this size do not exist, smoothing of the sensor signal was employed, by calculating an average of a given number of samples. Satisfactory results were obtained by taking the average of 50 sensor samples, as this reduced the noise level by 90%. Another source of noise, equally important to that of sensor noise, is due to the PWM amplifiers typically used in haptics. Placing the amplifier box 50 cm away from the device reduced the noise level to half of the initial one.

In conclusion, in low-force, soft environment applications of haptic devices, noise and device stiffness are the most important limiting factors in reducing force tracking errors. Stability analysis and unmodeled dynamics must be taken into account, but they tend not to be the limiting factors.

V. Conclusions

In this paper the effect of a force control law in the transparency of a low-force five degree-of-freedom (dof) haptic mechanism is investigated. Our effort focused on haptic devices, able to reproduce accurate, *low* forces in *soft* virtual environment, rather than stiff virtual walls. The mechanism, which is a part of a training medical simulator for urological operations, consists of a two-dof, five bar linkage and a three-dof spherical joint. Open and closed loop force control were described, simulated, experimentally studied, and compared. Stability conditions have been found using the Routh-Hurwitz criterion. These conditions are more strict than those in previous works. Simulation and experimental results of the force control law application on the five-dof mechanism were presented and discussed. It was found that the closed loop system exhibits substantially improved response with respect to the open loop system. Finally, it was shown that factors such as noise and device stiffness are more important than stability and environment stiffness in limiting the overall device fidelity.

References

[1] G. C. Burdea, *Force and touch feedback for virtual reality*, New York, NY: John Wiley and Sons, Inc., 1996.

[2] M. Minsky, M. Ouh-young, O. Steele, F. P. Brooks, Jr., and M. Behensky, "Feeling and Seeing: Issues in Force Display," *Computer Graphics,* vol. 24, no. 2, pp. 235-243, 1990.

[3] L. Birglen, C. Gosselin, N. Pouliot, B. Monsarrat, and T. Laliberté, "SHaDe, A New 3-DOF Haptic Device," *IEEE Transactions on Robotics and Automation,* vol. 18, no. 2, pp. 166-175, 2002.

[4] C. R. Carignan, and K. R. Cleary, "Closed-Loop Force Control for Haptic Simulation of Virtual Environments," *Haptics-e,* 1:2, 2000.

[5] R. Cortesão, J. Park, and O. Khatib, "Real-Time Adaptive Control for Haptic Manipulation with Active Observers," *Proc. IEEE/RSJ Int. Conference on Intelligent Robots and Systems*, Las Vegas, Nevada, 2003, pp. 2938-2943.

[6] J. E. Colgate, M. C. Stanley, and J. M. Brown, "Issues in the Haptic Display of Tool Use," *Proc. IEEE/RSJ Int. Conference on Intelligent Robots and Systems*, Pittsburgh, PA, 1995, pp. 140-145.

[7] C. B. Zilles and J. K. Salisbury, "A Constraint-Based God-Object Method for Haptic Display," *Proc. IEEE/RSJ Int. Conference on Intelligent Robots and Systems*, Pittsburgh, PA, 1995, 146-151.

[8] R. J. Adams, and B. Hannaford, "Stable Haptic Interaction with Virtual Environments," *IEEE Transactions on Robotics and Automation,* vol. 15, no. 3, pp. 465-474, 1999.

[9] R. J. Adams and B. Hannaford, "Control Law Design for Haptic Interfaces to Virtual Reality," *IEEE Transactions on Control Systems Technology,* vol. 10, no. 1, pp. 3-13, 2002.

[10] J. J. Gil, A. Avello, Á. Rubio, and J. Flórez, "Stability Analysis of a 1 DOF Haptic Interface Using the Routh-Hurwitz Criterion," *IEEE Tr. on Control Systems Technology,* vol. 12, no. 4, pp. 583-588, 2004.

[11] B. Hannaford, and J. Ryu, "Time-Domain Passivity Control of Haptic Interfaces," *IEEE Transactions on Robotics and Automation,* vol. 18, no. 1, pp. 1-10, 2002.

[12] B. E. Miller, J. E. Colgate, and R. A. Freeman, "Guaranteed Stability of Haptic Systems with Nonlinear Virtual Environments," *IEEE Tr. on Robotics and Automation,* vol. 16, no. 6, pp. 712-719, 2000.

[13] K. Vlachos, E. Papadopoulos, and D. N. Mitropoulos, "Design and implementation of a haptic device for training in urological operations," *IEEE Tr. on Robotics and Automation,* v. 19, no. 5, pp. 801-809, 2003.

[14] K. Vlachos and E. Papadopoulos, "Endpoint-Side Optimization of a Five Degree-of-Freedom Haptic Mechanism," *Proc. IEEE 13th Mediterranean Conference on Control and Automation*, Limassol, Cyprus, 2005, pp. 674-679.

[15] E. Papadopoulos, A. Tsamis, and K. Vlachos, "A Real-Time Graphic Environment for a Urological Operation Training Simulator," *Proc. IEEE Int. Conference on Robotics and Automation*, New Orleans, Louisiana, 2004, pp. 1295-1300.